Magn Reson Med Sci
doi:10.2463/mrms.mp.2022-0125 Published Online: December 16, 2022

MAJOR PAPER

Ex-vivo 1.5T MR Imaging versus CT in Estimating the Size of the Pathologically Invasive Component of Lung Adenocarcinoma Spectrum Lesions

Daisuke Yamada[1], Masaki Matsusako[1*], Daisuke Yoneoka[2], Katsunori Oikado[3], Hironori Ninomiya[4], Taiki Nozaki[1], Mitsutomi Ishiyama[3], Akari Makidono[5], Mizuto Otsuji[6], Harumi Itoh[7], and Hiroya Ojiri[8]

Purpose: The purpose of this study was to investigate whether *ex-vivo* MRI enables accurate estimation of the invasive component of lung adenocarcinoma.

Methods: We retrospectively reviewed 32 patients with lung adenocarcinoma who underwent lung lobectomy. The specimens underwent MRI at 1.5T. The boundary between the lesion and the normal lung was evaluated on a 5-point scale in each three MRI sequences, and a one-way analysis of variance and post-hoc tests were performed. The invasive component size was measured histopathologically. The maximum diameter of each solid component measured on CT and MR T1-weighted (T1W) images and the maximum size obtained from histopathologic images were compared using the Wilcoxon signed-rank test. Inter-reader agreement was evaluated using intraclass correlation coefficients (ICC).

Results: T1W images were determined to be optimal for the delineation of the lesions ($P < 0.001$). The histopathologic invasive area corresponded to the area where the T1W *ex-vivo* MR image showed a high signal intensity that was almost equal to the intravascular blood signal. The maximum diameter of the solid component on CT was overestimated compared with the maximum invasive size on histopathology (mean, 153%; $P < 0.05$), while that on MRI was evaluated mostly accurately without overestimation (mean, 108%; $P = 0.48$). The interobserver reliability of the measurements using CT and MRI was good (ICC = 0.71 on CT, 0.74 on MRI).

Conclusion: *Ex-vivo* MRI was more accurate than conventional CT in delineating the invasive component of lung adenocarcinoma.

Keywords: *ex-vivo magnetic resonance imaging, invasive component, lung adenocarcinoma, noninvasive alveolar collapse*

Introduction

Lung cancer, among the most common malignant neoplasms worldwide, is the leading cause of cancer-associated mortality in both sexes. The Fleischner Society's recommendations and findings of the Lung Cancer Screening Committee of the American College of Radiology Lung CT Screening Reporting and Data System suggest that the type and size of the nodule effectively indicate nodule management for reducing lung-cancer-specific mortality.[1–6]

The definition of the invasive component of lung adenocarcinoma remains under debate. According to the

[1]Department of Radiology, St. Luke's International University, Tokyo, Japan
[2]Infectious Disease Surveillance Center, National Institute of Infectious Diseases, Tokyo, Japan
[3]Diagnostic Imaging Center, The Cancer Institute Hospital of Japanese Foundation for Cancer Research, Tokyo, Japan
[4]Division of Pathology, The Cancer Institute Hospital of Japanese Foundation for Cancer Research, Tokyo, Japan
[5]Department of Diagnostic Radiology, Tokyo Metropolitan Children's Medical Center, Fuchu, Tokyo, Japan
[6]Department of Thoracic Surgery, Tokyo Metropolitan Bokutoh Hospital, Tokyo, Japan
[7]Department of Radiology, Faculty of Medical Sciences, University of Fukui, Yoshida-gun, Fukui, Japan
[8]Department of Radiology, The Jikei University School of Medicine and University Hospital, Tokyo, Japan
*Corresponding author: Department of Radiology, St. Luke's International Hospital, 9-1, Akashicho, Chuo-ku, Tokyo 104-8560, Japan. Phone: +81-3-3541-5151, Fax: +81-3-3541-5151, E-mail: makimatu@luke.ac.jp

Received: October 13, 2022 | Accepted: November 1, 2022

multidisciplinary classification of the International Association for the Study of Lung Cancer/American Thoracic Society/European Respiratory Society, a maximum dimension cut-off value of 0.5 cm for pathologically invasive components is a key criterion in differentiating invasive adenocarcinoma from minimally invasive adenocarcinoma (MIA). The invasive component size is significantly associated with survival.[7–10] Therefore, an image-based assessment of pathologically invasive components is desirable. Although CT-based evaluation of the invasive component of lung adenocarcinoma has been previously reported, the accurate detection of the extent of invasion by CT is often challenging[11,12] since the solid components on CT include myofibroblastic interstitium, alveolar collapse, fibrosis, inflammatory cell infiltration, and mucus retention, along with invasive foci in pathology.[13] The cut-off size for detecting invasion on CT could be larger than the actual size of the invasive component, and more accurate methods to measure the invasive diameter should be developed.

While the lung nodules have been commonly evaluated using CT, the clinical utility of MRI is fairly limited because of the rapid MR signal attenuation attributed to the inhomogeneity of the magnetic field. The latter is caused by the surrounding lung air and motion artifacts owing to low water content and cardiac and respiratory motion. Recently, new MRI techniques, such as pulmonary MRI with ultra-short TE (UTE-MRI), have been applied to lung diseases.[14–18] However, to the best of our knowledge, no study has reported on the detailed evaluation of the internal properties of lung cancer by high-resolution MRI.

This study aimed to investigate whether high-resolution *ex-vivo* MRI can accurately estimate the invasive component of lung adenocarcinoma by analyzing the characteristics of the signal intensity on MR images of each component of lung adenocarcinoma.

Materials and Methods

Ethics statement

This study was approved by the Institutional Review Board of St. Luke's International Hospital (approved no. 20-R016). The requirement of informed consent was waived owing to the retrospective nature of the study.

Patient population

The present study is a retrospective study using data from a previous study conducted at our institution. Prior to conducting this study, we obtained permission from our Ethics Review Committee to obtain comprehensive consent from the patients (approval number: 12-R025). As a requirement for secondary use, we again applied to the Research Review Board for approval (approval number: 20-R016). We used electronic medical records and picture archiving and communication system (PACS) to identify consecutive patients who underwent surgical resection to treat lung malignancies between December 2007 and February 2010. Patients who underwent lobectomy or total pneumonectomy were included. Those with a preoperative CT scan performed up to 3 months preoperatively and an MR scan performed on a postoperative specimen were also included. Patients who submitted a statement of nonparticipation, those who had not undergone a CT scan within 3 months prior to surgery, those who did not undergo an MRI scan of a postoperative formalin-fixed lung specimen, and those whose conditions were not histopathologically diagnosed as lung adenocarcinoma were excluded. Patient data were collected for 32 cases and 32 nodules (Fig. 1). In all patients, clinical and pathological classifications were determined based on the 2022 World Health Organization (Geneva) definitions.

Specimen processing

Formalin (20%) was injected into the lungs resected from the bronchial stump. A special hanging case and infuser were used for injecting formalin into the specimen under sufficient pressure. The direction of the injector tip was changed during injection to ensure uniform inflation of the entire specimen. A small syringe was used to inject additional formalin, after which a thin cap was inserted into the bronchial stump, closed, and finally sutured with silk sutures.

CT examination

All the CT images were acquired using a CT system (Aquilion; Canon Medical Systems, Tochigi, Japan) with the following parameters (120-kV tube voltage, 100–500 mA tube current, 32 mm collimation, 0.844 pitch, 320 mm FOV, and 512 × 512 matrix). Horizontal sectional slices were reconstructed at 5.0- and 1.0-mm intervals using the FC04, window width (WW): 350, window length (WL): 50 and filter convolution: 30, WW: 1500, and WL: −600 algorithms for the soft tissue and lung field conditions, respectively. Multiplanar reconstructions were acquired in coronal and sagittal planes at 2.5 mm intervals for the lung field conditions.

MRI examination

The formalin-injected resected lung was set to reproduce the *in-vivo* condition (supine position), and was stabilized with sponges. A 1-channel knee coil was used in a 1.5T imaging unit (Achieva; Philips Medical Systems, Best, the Netherlands). The imaging protocol was as follows: FOV, 20 cm; matrix, 512 × 512; slice thickness, 3 mm; number of excitations, 4; and T1-weighted (T1W; TR/TE 500/15), T2-weighted (T2W; TR/TE 5000/100), formalin attenuated inversion recovery images (FAIR) (TR/TE/ inversion time [TI] 11000/120/1800) were acquired. For FAIR images, the optimal TI to nullify the formalin signal was determined in advance. In the *ex-vivo* MR images, the normal parenchyma of the lungs was low signal intensity on T1W images, high signal intensity on T2W images, and low signal intensity on FAIR images. The intrapulmonary vessels revealed high signal intensity on T1W images, low signal intensity on T2W images, and high signal intensity on FAIR images (Fig. 2).

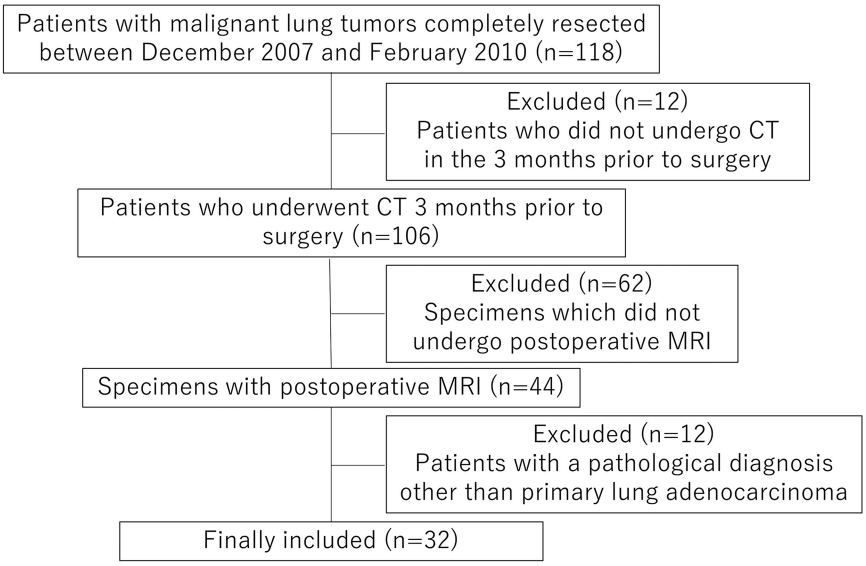

Fig. 1 Flowchart of patient selection and demographics. A flowchart of 118 consecutive patients who underwent surgery for malignant lung tumor resection at our hospital. Thirty-two patients were included.

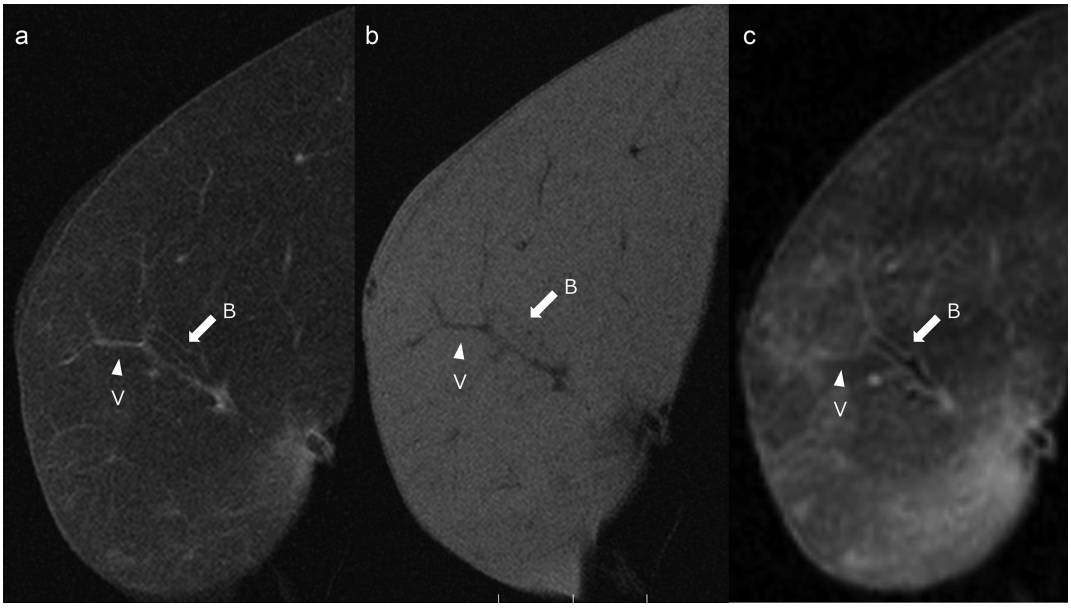

Fig. 2 Signal intensities of normal lung structures on *ex-vivo* MRI. (**a**) T1W image, (**b**) T2W image, (**c**) FAIR image. The normal lung parenchyma and bronchi (arrows) filled with formalin show a low signal intensity on the T1W image, a high signal intensity on the T2W image, and a low signal intensity on the FAIR image, which suppressed the formalin signal. The blood vessels in the lung show a high signal intensity on the T1W image, a low signal intensity on the T2W image, and a high signal intensity on the FAIR image (arrowheads). The blood vessels in the lungs show signal intensity that reflects the hematological components inside. B, bronchi; FAIR, formalin attenuated inversion recovery; T1W, T1-weighted; T2W, T2-weighted; V, blood vessel.

Correlation of preoperative CT and MR images of the resected lung specimen and histopathologic findings

The pathologic diagnosis of all 32 lesions was made by one pulmonary pathologist (with 15 years of experience), who classified the tumors according to the 2022 World Health Organization (Geneva) definitions and assessed the histologic growth pattern (lepidic, acinar, papillary, micropapillary, or solid pattern) to review the histopathologic aspects; percentages for each were tabulated at 5% intervals. Any histological type other than lepidic growth pattern was considered an invasive component.

In the 8th staging system, the size of the solid or invasive component is measured as the determinant of T factor. The size of the invasive foci was defined as the long axis diameter in accordance with the current pathology guidelines. For multiple invasive foci, the long axis diameter of the largest focus was used.

It was previously reported that the proliferation of active fibroblasts and destruction of the elastic fiber framework, which is the supporting structure of the alveoli, indicated tumor invasion.[19] Therefore, we pathologically assessed both the fibroblastic proliferation by hematoxylin and eosin staining and the elastic fiber framework by Elastica van Gieson staining. Noninvasive alveolar collapse was defined as a focus of the structural alveolar collapse with no active fibroblast proliferation and preserved elastic fiber skeleton, and its presence or absence was evaluated.[20]

Two observers (a thoracic radiologist with 8 years of experience and another thoracic radiologist with 36 years of experience) reviewed all CT and MRI findings. The readers evaluated the nodules on CT with a 1-mm slice and on MRI with a 3-mm slice. They rated the degree to which the boundary between the lesion and the normal lung was clearly demarcated in the three MRI sequences (T1W, T2W, and FAIR sequences) on a 5-point scale (5, Excellent; 4, Good; 3, Fair; 2, Poor; and 1, Failure).

Subsequently, referring to the pathologic findings, we determined by consensus which signal region in the MR image best matched the pathologic invasive area of the lung adenocarcinoma and defined this as the solid component in the MR image. After 3 months, the same observers independently measured the maximum diameter of the solid component on CT and MRI. The readings were obtained randomly to prevent recall bias. Discrepant cases were resolved by consensus.

The radiologic-pathologic invasiveness (RPI) ratio was defined as the maximum diameter of each solid component measured from CT and MRI divided by the maximum invasive diameter obtained from the histopathologic images, and the RPI ratio was calculated for each case.

Statistical analysis

A 5-point scale was employed to evaluate the lesion resolution of the three MRI sequences, and a one-way analysis of variance was used to determine the superior sequence. The Benjamini–Hochberg procedure was employed as a post-hoc test. The RPI ratio of the lesions measured from CT and MRI findings was evaluated for statistical significance using the Wilcoxon signed-rank sum test. The correlation coefficients between the maximum diameter of the solid component measured by CT and MRI and the diameter of the invasion on histopathology were calculated. The RPI ratios of the lesions with and without noninvasive alveolar collapse, measured by CT and MRI, were evaluated for statistical significance using the Wilcoxon signed-rank sum test. The inter-reader agreement was evaluated using the intraclass correlation coefficient (ICC). Statistical analysis was performed using the R statistical software (version 4.1.0; R Foundation for Statistical Computing, Vienna, Austria). $P < 0.05$ was considered statistically significant.

Results

Characteristics of the participants and tumors

Demographic data for the 32 study participants are shown in Table 1. The lobar location of the nodules was the right upper, right middle, right lower, left upper, and left lower lobe in 6, 3, 10, 7, and 6 cases, respectively. The overall nodule size was 26.49 ($\pm$ 11.69) mm on CT. The preoperative clinical N classification was N2 in only two patients. No distant metastases were observed.

Histopathologic characteristics of the tumors

The histologic characteristics of the 32 lung adenocarcinomas are shown in Table 1. The pathologic N classification was N2 in only two cases.

CT-MRI-pathologic correlation analysis

The mean score for lesion resolution for the three MRI sequences was 4.33 ($\pm$ 1.00) for the T1W images, 3.04 ($\pm$ 0.98) for T2W images, and 3.37 ($\pm$ 1.18) for FAIR images ($P < 0.001$). Consequently, we decided to use T1W images to measure the solid component of the lesions in this study. Furthermore, the high signal intensity area that was nearly the same as the intravascular blood signal in the T1W images was considered to reflect the pathological invasive areas most accurately (Fig. 3). The pathologically noninvasive alveolar collapse was clearly distinguished from the solid component on the T1W MR images, which showed a higher signal intensity than the normal lung and lower moderate signal intensity than the invasive area (Fig. 4).

Table 2 shows the size of the maximum invasion measured by CT, MRI, and histopathology. Pathologically invasive size was 12.36 $\pm$ 14.41 mm. The solid component size on CT was 18.92 $\pm$ 13.92 mm. The solid component size on MRI was 13.29 $\pm$ 13.91. The maximum diameter of the solid component measured by CT was an average of 153% larger than that measured by histopathology (RPI ratio = 1.53); an overestimation with statistical significance ($P < 0.05$) was noted. However, the maximum diameter of the MRI solid component was an average of 108% larger (RPI ratio = 1.08) ($P = 0.48$) (Table 2) (Fig. 5), with no significant difference from the size of the maximum invasion detected through pathologic diagnosis. The correlation coefficient between CT and pathology was r = 0.76, and that between MRI and histopathology was r = 0.93 (Fig. 6).

Table 3 shows the maximum diameter of invasion measured by CT, MRI, and histopathology, which were classified according to the alveolar collapse status. In the group with noninvasive alveolar collapse (n = 13), the pathologically invasive size was 7.50 $\pm$ 7.23 mm. The solid component

Table 1 The histologic characteristics of the 32 lung adenocarcinomas.

Characteristics	n (%)		
Age (mean±SD)	58.56±10.10		
Sex			
Male	16 (50%)		
Female	16 (50%)		
Smoking history			
Ever	22 (69%)		
Never	10 (31%)		
Type of nodules			
Ground-glass nodule	0 (0%)		
Part-solid nodule	22 (69%)		
Solid nodule	10 (31%)		
	Clinical T descriptoron CT	Clinical T descriptoron ex-vivo MRI	Pathologic T descriptor
Tis	0 (0%)	0 (0%)	3 (9%)
T1mi	2 (6%)	6 (6%)	4 (13%)
T1a	7 (22%)	10 (31%)	11 (34%)
T1b	13 (41%)	11 (34%)	8 (25%)
T1c	3 (9%)	3 (9%)	3 (9%)
T2a	5 (16%)	1 (3%)	2 (6%)
T2b	1 (3%)	0 (0%)	0 (0%)
T3	0 (0%)	0 (0%)	0 (0%)
T4	1 (3%)	1 (3%)	1 (3%)
Histologic type	n (%)		
AIS	4 (13%)		
MIA	4 (13%)		
Lepidic-predominant IA	9 (28%)		
Acinar-predominant IA	1 (3%)		
Papillary-predominant IA	9 (28%)		
Micropapillary-predominant IA	3 (9%)		
Solid-predominant IA	2 (6%)		
Pleural invasion	4 (13%)		
Lymphatic invasion	6 (19%)		
Venous invasion	6 (19%)		

AIS, adenocarcinoma in situ, IA, invasive adenocarcinoma; MIA, minimally invasive adenocarcinoma; SD, standard deviation.

size on CT was 20.17 ± 11.71 mm, while that on MRI was 9.28 ± 5.17. The maximum diameter of the solid component on CT was significantly overestimated by an average of 269% (RPI ratio = 2.69) compared with the maximum invasion diameter on histopathology ($P < 0.05$). In contrast, the maximum diameter of the MRI solid component was measured an average of 124% larger (RPI ratio = 1.24) ($P = 0.18$) (Table 3) (Fig. 7a) without any significant

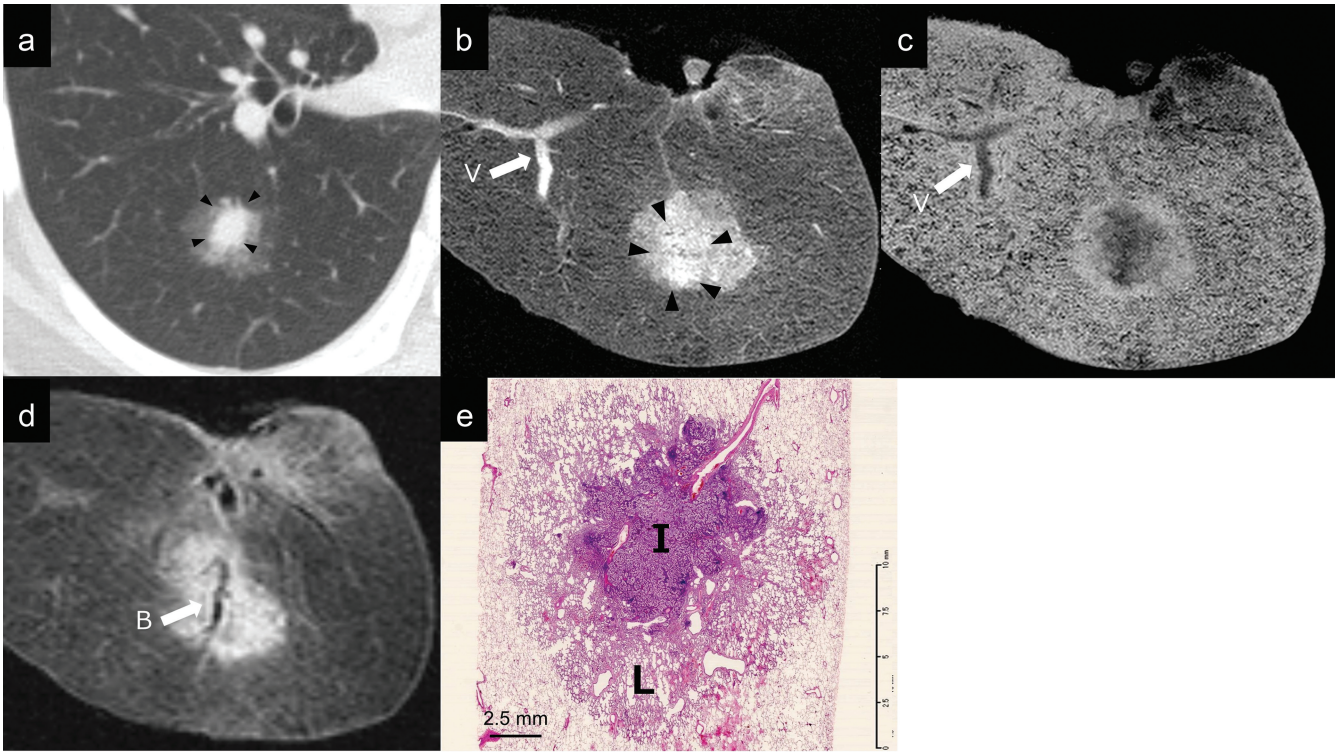

Fig. 3 Part-solid nodule on *ex-vivo* MRI. Images of a 49-year-old woman diagnosed with lung adenocarcinoma of the right lower lung. (**a**) There is a part-solid nodule with an overall diameter of 23 mm and a solid component of 16 mm (arrowheads) in the lower lobe of the right lung on the CT image. (**b**) The region corresponding to the solid component on CT shows the same level of high signal intensity as the blood vessels (arrow) on the T1W image (arrowheads). (**c**) The region corresponding to the solid component on CT shows the same inhomogeneously low signal intensity as the blood vessels (arrow) on the T2W image. (**d**) The nodule shows higher signal intensity compared to bronchi (arrow) on the FAIR image. (**e**) Histologically, the patient was diagnosed as having lepidic predominant non-mucinous adenocarcinoma (60% lepidic, 40% micropapillary). This tumor consists primarily of L with a central I (hematoxylin-eosin stain). Panels **a**–**c** show slices from the same level, and **d** shows a slice from the level of 6 mm to the caudal side than **a**–**c**. B, bronchi; FAIR, formalin attenuated inversion recovery; I, area of invasion; L, lepidic growth of tumor cells; T1W, T1-weighted; T2W, T2-weighted; V, blood vessel.

difference. In the group without noninvasive alveolar collapse (n = 19), pathologically invasive size was 12.36 ± 16.94 mm. The solid component size on CT was 18.06 ± 15.19 mm, while that on MRI was 16.03 ± 17. The maximum diameter of the solid component on CT was measured an average of 115% larger than the maximum invasiveness size on physical histology without any significant difference (RPI ratio = 1.15) ($P = 0.16$). Similarly, the maximum diameter of the MRI solid component was measured as an average of 102% larger without any significant difference compared to the maximum invasion diameter by histopathology (RPI ratio = 1.02) ($P = 0.86$) (Table 3) (Fig. 7b). The inter-reader agreement was favorable with ICCs 0.71 and 0.74 on CT and MRI, respectively.

Discussion

In this study, the areas that were considered to most accurately reflect the pathologically invasive area were those that showed a high signal intensity, nearly as high as the intravascular blood signal in the T1W MR images. The maximum diameter of the solid component on CT was significantly overestimated by an average of 153% compared to the maximum diameter of the invasion on histopathology, whereas the maximum diameter of the solid component on MRI was nearly correct, measuring an average of 108% larger. In particular, the invasion area was significantly overestimated on CT, especially when noninvasive alveolar collapse was present, while a more accurate diagnosis was possible with MRI. Noninvasive alveolar collapse was also depicted as a solid component on CT, which did not accurately reflect the pathologic diameter of the invasion, suggesting that MRI would be able to distinguish noninvasive collapse from the invasive area. These results suggest that the preoperative staging of the International Association for the Study of Lung Cancer (IASLC) classification tends to be lower when assessed by *ex-vivo* MRI than by CT scan, and is more similar to postoperative pathology.

On *ex-vivo* MRI, the areas of lung adenocarcinoma that pathologically show a lepidic growth pattern presumably show a relatively lower signal intensity on T1W images than the invasive areas as they are filled with formalin,

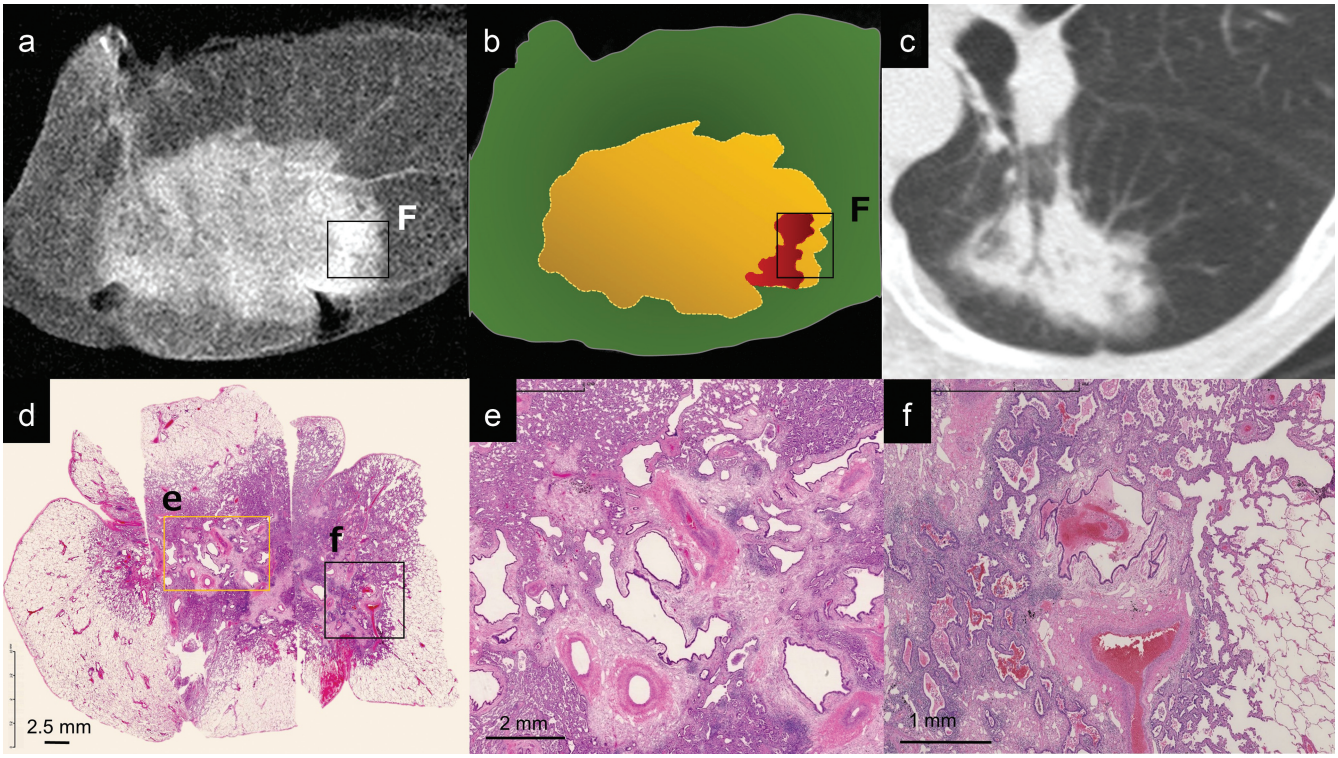

Fig. 4 Lung adenocarcinoma with noninvasive alveolar collapse on *ex-vivo* MRI. Images of a 69-year-old man diagnosed with adenocarcinoma of the lung with noninvasive alveolar collapse. (**a**) Most of the lesions show heterogeneous intermediate signal intensity; however, there is a localized area of high signal intensity at the edge of the left side of the T1W image. (**b**) This is a schema of the T1W image. The green, yellow, and red areas show the normal lung, intermediate-signal areas, and high-signal areas on the T1W image, respectively. The area enclosed by the square is the area corresponding to histopathologic image (**f**). (**c**) Most of the lesions are occupied by solid components on the CT image. (**d**) Histologically, non-mucinous adenocarcinoma (lepidic 70%, papillary 25%, micropapillary 5%) is diagnosed. Most of the lesion consists of areas of lepidic growth of tumor cells with noninvasive alveolar collapse, and the invasive foci are only observed at the left edge of the lesion (hematoxylin-eosin stain). (**e**) Low-magnification photomicrograph shows areas of lepidic growth of tumor cells with noninvasive alveolar collapse that represent most of the lesion. (**f**) Low-magnification photomicrograph shows the border area between the invasive lesion observed on the left edge of the lesion and the normal lung. T1W, T1-weighted.

Table 2 Comparison of CT, MRI, and pathologically invasive size.

	Diameter (mm)	Average RPI ratio	*P*
Pathologically invasive size (mean ± SD)	12.36 ± 214.41**		
Solid component size on MRI (mean ± SD)	13.29 ± 199.73	1.08	0.48
Solid component size on CT (mean ± SD)	18.92 ± 200.16	1.53	< 0.05*

*$P < 0.05$. **standard reference. RPI, radiologic-pathologic invasiveness; SD, standard deviation.

which produces a low signal intensity on T1W images. In contrast, the invasive areas of lung adenocarcinoma show a high signal intensity on T1W images because the invasive areas are completely devoid of air content; therefore, there is no formalin to fill them, which could attribute to the relatively high signal intensity on T1W images.

Here, *ex-vivo* MRI demonstrated the potential to determine the size of the invasive component of lung adenocarcinoma more accurately than conventional CT, possibly because *ex-vivo* MRI has better contrast resolution than CT and provides better spatial resolution by increasing the in-plane resolution and the number of excitations, which improves the spatial resolution and enables a detailed depiction of the lung microstructure. The CT measurement diameter may be larger than the accurate size of the invasive component, which is consistent with the results of this study, as the invasive area, collapse, and fibrosis are all depicted uniformly as solid components without tissue

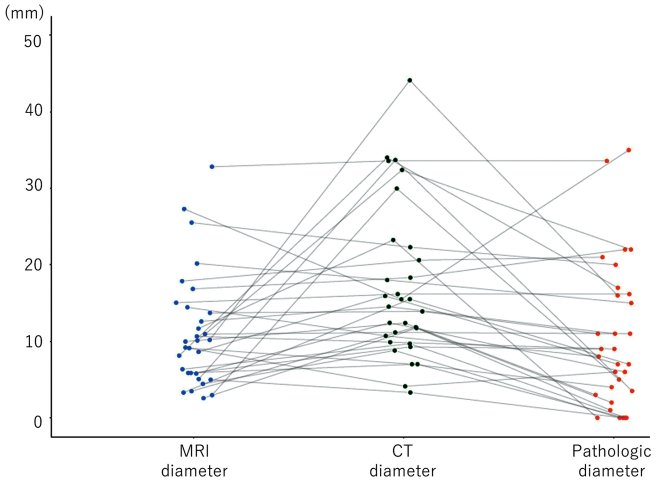

Fig. 5 Scatter plot showing direct comparisons of the pathologically invasive size with largest dimensions of solid components on CT and those on MRI. The blue dots show the maximum diameter of the solid component of the lesion on MRI in each case. The green and orange dots show the maximum diameter of the solid component of the lesion on CT and the diameter of the invasion on histopathology, respectively.

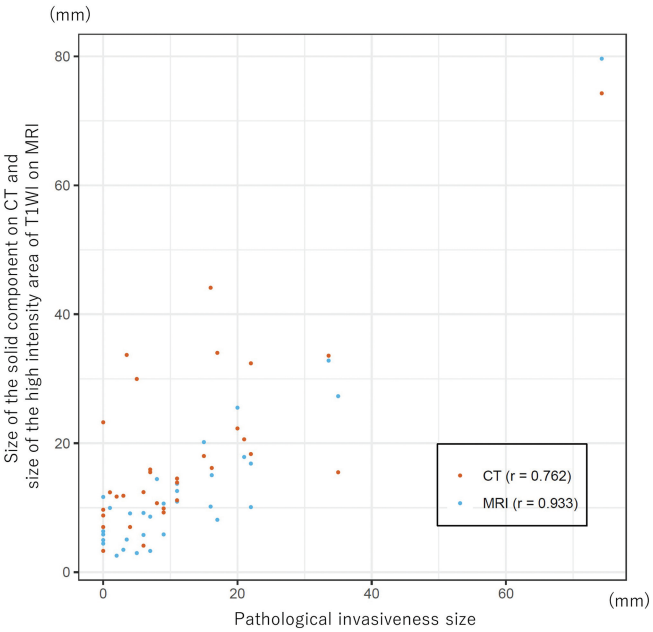

Fig. 6 Scatter plot and correlation coefficient showing direct comparisons of the pathologically invasive size with largest dimensions of solid components on CT and those on MRI. The blue dots show direct comparisons of pathologically invasive size with largest dimensions of the solid components on MRI. The orange dots show direct comparisons of the pathologically invasive size with largest dimensions of solid components on CT. The correlation coefficient between CT and pathology was r = 0.76, and that between MRI and histopathology was r = 0.93.

Table 3 Comparison of CT, MRI, and pathologically invasive size with or without noninvasive alveolar collapse.

	With noninvasive alveolar collapse (n = 13)			Without noninvasive alveolar collapse (n = 19)		
	Diameter (mm)	Average RPI ratio*	*P*	Diameter (mm)	Average RPI ratio*	*P*
Pathologically invasive size (mean ± SD)	7.50 ± 56.58**			12.36 ± 214.41**		
Solid component size on MRI (mean ± SD)	9.28 ± 29.14	1.24	0.33	16.03 ± 305.06	1.02	0.86
Solid component size on CT (mean ± SD)	20.17 ± 148.54	2.69	< 0.05*	18.06 ± 243.78	1.15	0.16

*$P < 0.05$. **standard reference. RPI, radiologic-pathologic invasiveness; SD, standard deviation.

contrast on CT.[13,21] In the present study, MRI was superior to CT, especially in differentiating the noninvasive alveolar collapse from the invasive component of lung adenocarcinoma.

Several studies have been conducted on *ex-vivo* MR images in other cancer types.[22–25] Heitzman's fixation method, the specimen processing method adapted in this study, has been used for radiologic-pathologic correlation in various investigations to better understand the relationship between lung disease and lung anatomy. However, it has been limited to radiography and CT for both purposes.[26,27] No studies, to date, have used *ex-vivo* MRI in lung cancer research. Early detection of lung cancer and characterization of lung nodules are important challenges in radiology, and, to date, this role has been dominated by CT; however, UTE, a new sequence, has demonstrated that MRI can nearly compete with CT in lung nodule detection.[14,15] Although this study involved *ex-vivo* MR examination, its results suggest that MRI may allow for a detailed analysis of the internal properties of lung cancer. Recently, not only conventional CT but also PET/CT and PET/MRI have been utilized for lung cancer staging in clinical practice.[28,29] In addition, whole-body MRI, which can evaluate the size of local invasion, the presence or absence of lymph node metastases,

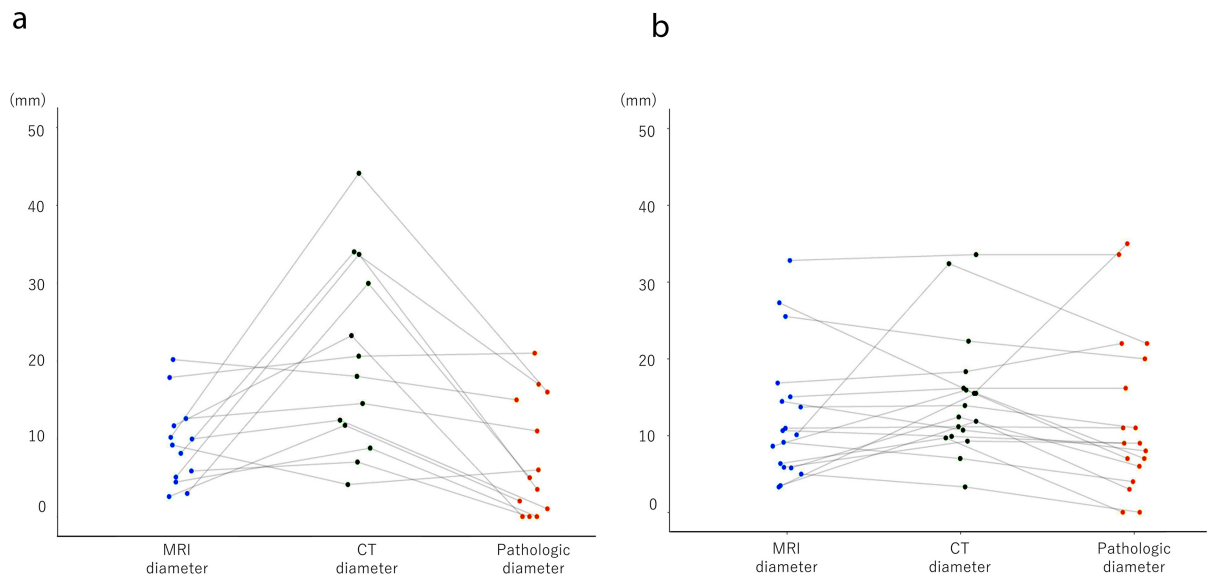

Fig. 7 Scatter plot showing direct comparisons of the pathologically invasive size with largest dimensions of solid components on CT and those on MRI divided by the presence or absence of noninvasive alveolar collapse. The blue dots show the maximum diameter of the solid components of the lesion on MRI in each case. The green dots show the maximum diameter of the solid component of the lesion on CT, while the orange dots show the diameter of the invasion on histopathology. (**a**) The specimens with noninvasive alveolar collapse and (**b**) the specimens without noninvasive alveolar collapse are presented.

and the presence or absence of metastases in other organs, is now being studied for cancer staging.[30] In the future, the usefulness of MRI will be further demonstrated in the treatment of lung cancer. We believe that our study will be a cornerstone of MRI research, especially with regard to tumor invasion.

Limitations

This study has several limitations. First, it is a single-center, retrospective study; hence, selection bias may exist. Second, few cases were included, and more patients with invasive tumors than noninvasive tumors were included as we recruited patients who had undergone surgery for lung cancer. Third, the study utilized *ex-vivo* MR images of tissue specimens with formalin, and respiratory motion or time constraints were absent. Specifically, as the imaging methods and conditions are different from those of actual *in-vivo* MR images, the present imaging sequence cannot be applied directly to *in-vivo* MR images. Fourth, the latest MRI technology was not used, and determination of the invasive component was limited to the evaluation of T1W images only. Nevertheless, the study of the most basic sequence and T1W and T2W images would be useful in future MRI studies.

Conclusion

We could more accurately delineate the invasive component of lung adenocarcinoma with *ex-vivo* MRI than with conventional CT. In particular, the present study showed the possibility that MRI would be able to distinguish noninvasive collapse from the invasive area. MRI has the potential to more accurately delineate the invasive component in pulmonary nodules and to reflect more accurate staging. Therefore, further studies using *in-vivo* MRI are needed. In the future, MRI may be useful in the analysis of the internal characteristics of lung cancer in clinical practice.

Conflicts of Interest

The authors declare that they have no conflicts of interest.

References

1. MacMahon H, Austin JH, Gamsu G, et al. Guidelines for management of small pulmonary nodules detected on CT scans: a statement from the Fleischner Society. Radiology 2005; 237:395–400.
2. Naidich DP, Bankier AA, MacMahon H, et al. Recommendations for the management of subsolid pulmonary nodules detected at CT: a statement from the Fleischner Society. Radiology 2013; 266:304–317.
3. Kazerooni EA, Armstrong MR, Amorosa JK, et al. ACR CT accreditation program and the lung cancer screening program designation. J Am Coll Radiol 2015; 12:38–42.
4. MacMahon H, Naidich DP, Goo JM, et al. Guidelines for management of incidental pulmonary nodules detected on CT images: from the Fleischner Society 2017. Radiology 2017; 284:228–243.
5. American College of Radiology, Lung-Screening Reporting and Data System. (LungRADS) Version 1.1, 2019. https://www.acr.

org/-/media/ACR/Files/RADS/Lung-RADS/LungRADSAssessmentCategoriesv1-1.pdf. (Accessed: March 3, 2022)
6. Dyer SC, Bartholmai BJ, Koo CW. Implications of the updated Lung CT Screening Reporting and Data System (Lung-RADS version 1.1) for lung cancer screening. J Thorac Dis 2020; 12:6966–6977.
7. Borczuk AC, Qian F, Kazeros A, et al. Invasive size is an independent predictor of survival in pulmonary adenocarcinoma. Am J Surg Pathol 2009; 33:462–469.
8. Yim J, Zhu LC, Chiriboga L, Watson HN, Goldberg JD, Moreira AL. Histologic features are important prognostic indicators in early stages lung adenocarcinomas. Mod Pathol 2007; 20:233–241.
9. Maeshima AM, Tochigi N, Yoshida A, Asamura H, Tsuta K, Tsuda H. Histological scoring for small lung adenocarcinomas 2 cm or less in diameter: a reliable prognostic indicator. J Thorac Oncol 2010; 5:333–339.
10. Tsutani Y, Miyata Y, Mimae T, et al. The prognostic role of pathologic invasive component size, excluding lepidic growth, in stage I lung adenocarcinoma. J Thorac Cardiovasc Surg 2013; 146:580–585.
11. Lee HJ, Lee CH, Jeong YH, et al. IASLC/ATS/ERS International Multidisciplinary Classification of Lung Adenocarcinoma: novel concepts and radiologic implications. J Thorac Imaging 2012; 27:340–353.
12. Lee SM, Park CM, Goo JM, Lee HJ, Wi JY, Kang CH. Invasive pulmonary adenocarcinomas versus preinvasive lesions appearing as ground-glass nodules: differentiation by using CT features. Radiology 2013; 268:265–273.
13. Austin JH, Garg K, Aberle D, et al. Radiologic implications of the 2011 classification of adenocarcinoma of the lung. Radiology 2013; 266:62–71.
14. Ohno Y, Koyama H, Yoshikawa T, et al. Pulmonary high-resolution ultrashort TE MR imaging: comparison with thin-section standard- and low-dose computed tomography for the assessment of pulmonary parenchyma diseases. J Magn Reson Imaging 2016; 43:512–532.
15. Ohno Y, Koyama H, Yoshikawa T, et al. Standard-, reduced-, and no-dose thin-section radiologic examinations: comparison of capability for nodule detection and nodule type assessment in patients suspected of having pulmonary nodules. Radiology 2017; 284:562–573.
16. Wielpütz MO, Lee HY, Koyama H, et al. Morphologic characterization of pulmonary nodules with ultrashort TE MRI at 3T. AJR Am J Roentgenol 2018; 210:1216–1225.
17. Zhu X, Chan M, Lustig M, Johnson KM, Larson PEZ. Iterative motion-compensation reconstruction ultra-short TE (iMoCo UTE) for high-resolution free-breathing pulmonary MRI. Magn Reson Med 2020; 83:1208–1221.
18. Noguchi M, Morikawa A, Kawasaki M, et al. Small adenocarcinoma of the lung. Histologic characteristics and prognosis. Cancer 1995; 75:2844–2852.
19. Zeng F, Nogami M, Ueno YR, et al. Diagnostic performance of zero-TE lung MR imaging in FDG PET/MRI for pulmonary malignancies. Eur Radiol 2020; 30:4995–5003.
20. Inafuku K, Yokose T, Ito H, et al. Should pathologically non-invasive lung adenocarcinoma larger than 3 cm be classified as T1a. Ann Thorac Surg 2019; 108:1678–1684.
21. Yanagawa M, Kusumoto M, Johkoh T, et al. Radiologic-pathologic correlation of solid portions on thin-section CT images in lung adenocarcinoma: a multicenter study. Clin Lung Cancer 2018; 19:e303–e312.
22. Inoue A, Ohta S, Nitta N, et al. Ex vivo MR imaging of colorectal carcinoma before and after formalin fixation: correlation with histopathologic findings. Abdom Radiol (NY) 2018; 43:1524–1530.
23. Heidkamp J, Zusterzeel PLM, van Engen-van Grunsven ACH, et al. MRI evaluation of vulvar squamous-cell carcinoma in fresh radical local excision specimens for cancer localization and prediction of surgical tumor-free margins. NMR Biomed 2019; 32:e4025.
24. Bailey C, Siow B, Panagiotaki E, et al. Microstructural models for diffusion MRI in breast cancer and surrounding stroma: an ex vivo study. NMR Biomed 2017; 30:e3679.
25. Heidkamp J, Hoogenboom M, Kovacs IE, et al. Ex vivo MRI evaluation of prostate cancer: localization and margin status prediction of prostate cancer in fresh radical prostatectomy specimens. J Magn Reson Imaging 2018; 47:439–448.
26. Heitzman ER. Bronchogenic carcinoma: radiologic-pathologic correlations. Semin Roentgenol 1977; 12:165–174.
27. Itoh H, Tokunaga S, Asamoto H, et al. Torizuka, Radiologic-pathologic correlations of small lung nodules with special reference to peribronchiolar nodules. AJR Am J Roentgenol 1978; 130:223–231.
28. Ehman EC, Johnson GB, Villanueva-Meyer JE, et al. PET/MRI: where might it replace PET/CT? J Magn Reson Imaging 2017; 46:1247-1262.
29. Sawicki LM, Grueneisen J, Buchbender C, et al. Evaluation of the outcome of lung nodules missed on 18F-FDG PET/MRI compared with 18F-FDG PET/CT in patients with known malignancies. J Nucl Med 2016; 57:15–20.
30. Taylor SA, Mallett S, Ball S, et al. Diagnostic accuracy of whole-body MRI versus standard imaging pathways for metastatic disease in newly diagnosed non-small-cell lung cancer: the prospective Streamline L trial. Lancet Respir Med 2019; 7:523-532.